Full paper

CONTRAST MEDIA & MOLECULAR IMAGING

Received: 29 January 2016, Accepted: 9 March 2016, Published online in Wiley Online Library

(wileyonlinelibrary.com) DOI: 10.1002/cmmi.1696

Sortase A-mediated site-specific labeling of camelid single-domain antibody-fragments: a versatile strategy for multiple molecular imaging modalities

Sam Massa[a,b], Niravkumar Vikani[b], Cecilia Betti[c], Steven Ballet[c], Saskia Vanderhaegen[d,e], Jan Steyaert[d,e], Benedicte Descamps[f], Christian Vanhove[f], Anton Bunschoten[g], Fijs W. B. van Leeuwen[g], Sophie Hernot[a], Vicky Caveliers[a,h], Tony Lahoutte[a,h], Serge Muyldermans[b], Catarina Xavier[a]*,†and Nick Devoogdt[a,b]*,†

A generic site-specific conjugation method that generates a homogeneous product is of utmost importance in tracer development for molecular imaging and therapy. We explored the protein-ligation capacity of the enzyme Sortase A to label camelid single-domain antibody-fragments, also known as nanobodies. The versatility of the approach was demonstrated by conjugating independently three different imaging probes: the chelating agents CHX-A"-DTPA and NOTA for single-photon emission computed tomography (SPECT) with indium-111 and positron emission tomography (PET) with gallium-68, respectively, and the fluorescent dye Cy5 for fluorescence reflectance imaging (FRI). After a straightforward purification process, homogeneous single-conjugated tracer populations were obtained in high yield (30–50%). The enzymatic conjugation did not affect the affinity of the tracers, nor the radiolabeling efficiency or spectral characteristics. *In vivo*, the tracers enabled the visualization of human epidermal growth factor receptor 2 (HER2) expressing BT474M1-tumors with high contrast and specificity as soon as 1 h post injection in all three imaging modalities. These data demonstrate Sortase A-mediated conjugation as a valuable strategy for the development of site-specifically labeled camelid single-domain antibody-fragments for use in multiple molecular imaging modalities. Copyright © 2016 John Wiley & Sons, Ltd.

Additional supporting information can be found in the online version of this article at the publisher's website.

Keywords: chemoenzymatic ligation; HER2; multimodal; nanobody; sdAb; site-specific conjugation; Sortase A

* *Correspondence to: C. Xavier and N. Devoogdt, Vrije Universiteit Brussel, Laarbeeklaan 103, building K, 1090 Brussels, Belgium. E-mail: cxavier@vub.ac.be; ndevoogd@vub.ac.be*

† *These authors share senior authorship.*

a *S. Massa, S. Hernot, V. Caveliers, T. Lahoutte, C. Xavier, N. Devoogdt In vivo Cellular and Molecular Imaging laboratory, Vrije Universiteit Brussel (VUB), 1090, Brussels, Belgium*

b *S. Massa, N. Vikani, S. Muyldermans, N. Devoogdt Laboratory of Cellular and Molecular Immunology, Vrije Universiteit Brussel (VUB), 1050, Brussels, Belgium*

c *C. Betti, S. Ballet Laboratory of Organic Chemistry, Vrije Universiteit Brussel (VUB), 1050, Brussels, Belgium*

d *S. Vanderhaegen, J. Steyaert Structural Biology Brussels, Vrije Universiteit Brussel (VUB), 1050, Brussels, Belgium*

e *S. Vanderhaegen, J. Steyaert Structural Biology Research Center, VIB, 1050, Brussels, Belgium*

f *B. Descamps, C. Vanhove Infinity-MEDISIP-iMinds Medical IT, Department of Electronics and Information Systems, Ghent University, 9000, Ghent, Belgium*

g *A. Bunschoten, F. W. B. van Leeuwen Interventional Molecular Imaging Laboratory, Department of Radiology, Leiden University Medical Center, 2333ZA, Leiden, The Netherlands*

h *V. Caveliers, T. Lahoutte Nuclear Medicine Department, Universitair Ziekenhuis Brussel, Vrije Universiteit Brussel (VUB), 1090, Brussels, Belgium*

Abbreviations: *CT, X-ray computed tomography; ESI-Q-ToF, electrospray ionization quadrupole time-of-flight; FRI, fluorescence reflectance imaging; HER2, human epidermal growth factor receptor 2; His-tag, hexahistidine-tag; IMAC, immobilized metal affinity chromatography; iTLC, instant thin-layer chromatography; LDS-PAGE, lithium dodecyl sulphate polyacrylamide gel electrophoresis; MRI, magnetic resonance imaging; PET, positron emission tomography; RP-HPLC, reverse-phase HPLC; scFv, single-chain variable fragment; sdAb, camelid single-domain antibody-fragment; SEC, size-exclusion chromatography; sortag, Sortase A recognition motif; SPECT, single-photon emission computed tomography; SPR, surface plasmon resonance; SrtA, Sortase A; % IA/g, percentage of injected activity per gram of tissue*

1. INTRODUCTION

The conjugation of a label to a targeting agent is a pivotal step in the generation of high quality imaging tracers and therapeutic agents. The classical methods for protein conjugation to the side chain ε-amine group of lysine residues or sulfhydryl group of cysteine residues are often applied, but have their limitations. Antibodies and antibody-derived fragments usually have several solvent-exposed lysines making it difficult to control where and how many labels will be conjugated (1). Moreover, the occurrence of a lysine residue in or near the antigen-binding site can lead to impairment of the targeting agent upon conjugation (2,3). The resulting heterogeneous tracer populations can be avoided by, alternatively, introducing an unpaired cysteine within the targeting agent for site-specific conjugation. However, this strategy requires a reduction step with careful titration of the reducing agent, to liberate the introduced cysteine residue without reducing intradomain disulfide bonds that are crucial for stability, and which can result in unwanted reduction side-products (4,5).

Several alternatives for site-specific conjugation are being investigated, including the modification of glycans, the incorporation of unnatural amino acids, and the use of chemoenzymatic reactions (6). In this work we explored the use of Sortase A (SrtA), a transpeptidase derived from *Staphylococcus aureus* that naturally catalyses the anchoring of cell wall proteins to the peptidoglycan layer of the bacterial cell (7). Gradually the recombinant form of the enzyme found its way into many biotechnological applications because of the straightforward introduction of a bioorthogonal functionality into a protein-of-interest (8–10). The transpeptidation follows a two-step reaction mechanism (Fig. 1A). First, SrtA cleaves the polypeptide backbone of the substrate protein at the position where the SrtA recognition motif (sortag) LPXTG was incorporated, with formation of an acyl-enzyme intermediate. Subsequently, a new peptide bond is formed between the threonine residue in the sortag and the *N*-terminal glycine of a nucleophilic probe, containing the bioorthogonal functionality. Key advantages of the system are: the simple production of the recombinant enzyme in substantial amounts, its flexibility towards its substrates, and the required presence of only very short peptides in these substrates (the sortag LPXTG in the target protein and a nucleophilic *N*-terminal oligoglycine within the biorthogonal probe).

Here we describe a generic strategy for SrtA-mediated site-specific labeling of camelid single-domain antibody-fragments (sdAbs) to develop proficient reagents for non-invasive, *in vivo* molecular imaging and therapy. A sdAb, also called V_HH or nanobody, is the recombinantly isolated antigen-binding domain of heavy-chain-only antibodies that occur in species of the *Camelidae* family (11). Its small size (12–15 kDa) and high specificity and affinity for its cognate antigen make it a successful targeting agent for diagnostic imaging and targeted radionuclide therapy (12–14). Since a variety of radioisotopes and fluorescent dyes are available, access to a generic conjugation strategy is highly desired. The use of SrtA-mediated conjugation for the site-specific labeling of sdAbs was demonstrated by functionalizing the human epidermal growth factor receptor 2 (HER2)-targeting sdAb 2Rs15d independently with three different labels. The functionality of the new tracer constructs was subsequently validated *in vitro* and *in vivo* in tumor-targeting experiments with multiple imaging modalities.

2. RESULTS

2.1. Design of the reaction substrates

The use of SrtA to conjugate a bioorthogonal probe to a protein-of-interest requires only limited adaptations of these reaction substrates. The target protein needs to possess a sortag (LPXTG) at the desired conjugation site and the bioorthogonal probe, in this case a chelating agent or fluorescent dye, needs to contain a nucleophilic *N*-terminal glycine. The enzyme itself is produced as a hexahistidine-tagged (His-tagged) recombinant protein (Supplementary material and methods).

We explored the SrtA-mediated labeling strategy with the HER2-targeting sdAb 2Rs15d and the non-targeting control sdAb BcII10 as model compounds. Both sdAbs were expressed with a *C*-terminal sortag (LPETG), followed by a His-tag (Fig. 1A). The His-tag facilitates the purification of the sdAb via immobilized metal affinity chromatography (IMAC) during production, but is eliminated upon SrtA-mediated cleavage.

To demonstrate the versatility of SrtA-mediated conjugation in the context of molecular imaging, we synthesized three different nucleophilic imaging probes containing the chelating agents CHX-A"-DTPA or NOTA, for use in single-photon emission computed tomography (SPECT) and positron emission tomography (PET), respectively, or the fluorescent dye Cy5 (excitation: 650 nm, emission: 670 nm), for use in fluorescence reflectance imaging (FRI) (Fig. 2) (Supplementary material and methods). In a first step the pentapeptide H-GGGYK-NH_2 was synthesized using standard solid phase peptide synthesis. Besides the *N*-terminal triglycine, we included a tyrosine residue for its UV absorbance property at 280 nm and a lysine residue for attachment of the chelating agent or fluorescent dye. Next, we conjugated CHX-A"-DTPA-NCS, NOTA-NCS or Cy5 to the side chain ε-amine of the lysine residue of the pentapeptide. The resulting nucleophilic imaging probes were purified via reverse-phase HPLC (RP-HPLC) and subsequently lyophilized.

2.2. SrtA-mediated conjugation

The SrtA-mediated conjugation was optimized with sdAb 2Rs15d-sortag and CHX-A"-DTPA as the substrates. The sdAb concentration was kept constant while the SrtA and imaging probe concentrations, as well as the reaction time were varied (Fig. S1). To evaluate the reaction efficiency, advantage was taken from the elimination of the His-tag upon conjugation. In an anti-His-tag Western blot the consumption of sdAb starting product is visualized by a decreasing intensity of the sdAb band. An overnight reaction with a molar ratio sdAb : SrtA : nucleophilic imaging probe of 1:3:30 was found most optimal. Consequently this condition was used for conjugation of the three nucleophilic imaging probes. For each of the probes the reaction efficiency was determined in Western blot (Fig. 3). Comparison of the intensity of the sdAb band in lane 3 (reaction mixture with all three components) to lane 1 (reference lane with only sdAb) indicated that the chemo-enzymatic reaction consumed at least 75% of the sdAb substrate, regardless the imaging probe used. In a control reaction sdAb and SrtA were incubated without the imaging probe (lane 2). In this case the reaction could not proceed beyond the acyl-enzyme intermediate (SrtA bound to sdAb), resulting in a more intense band of the intermediate (visible by the His-tag of SrtA) and less consumption of the sdAb substrate. In the case of Cy5, the final conjugated product Cy5-2Rs15d could also be visualized in the 700 nm-channel.

2.3. Purification of the conjugated sdAbs

Besides the conjugated sdAb, the reaction mixture still contains unreacted sdAb and imaging probe, SrtA, as well as acyl-enzyme intermediate and released His-tag that result from the first step of the conjugation reaction. Therefore the purification protocol consisted of (i) IMAC, to remove all undesired His-tagged products, (ii) EDTA competition, to prevent occupation of the chelating agents by Ca^{2+} or Ni^{2+} ions, and (iii) size-exclusion chromatography (SEC), to separate the conjugated sdAb from

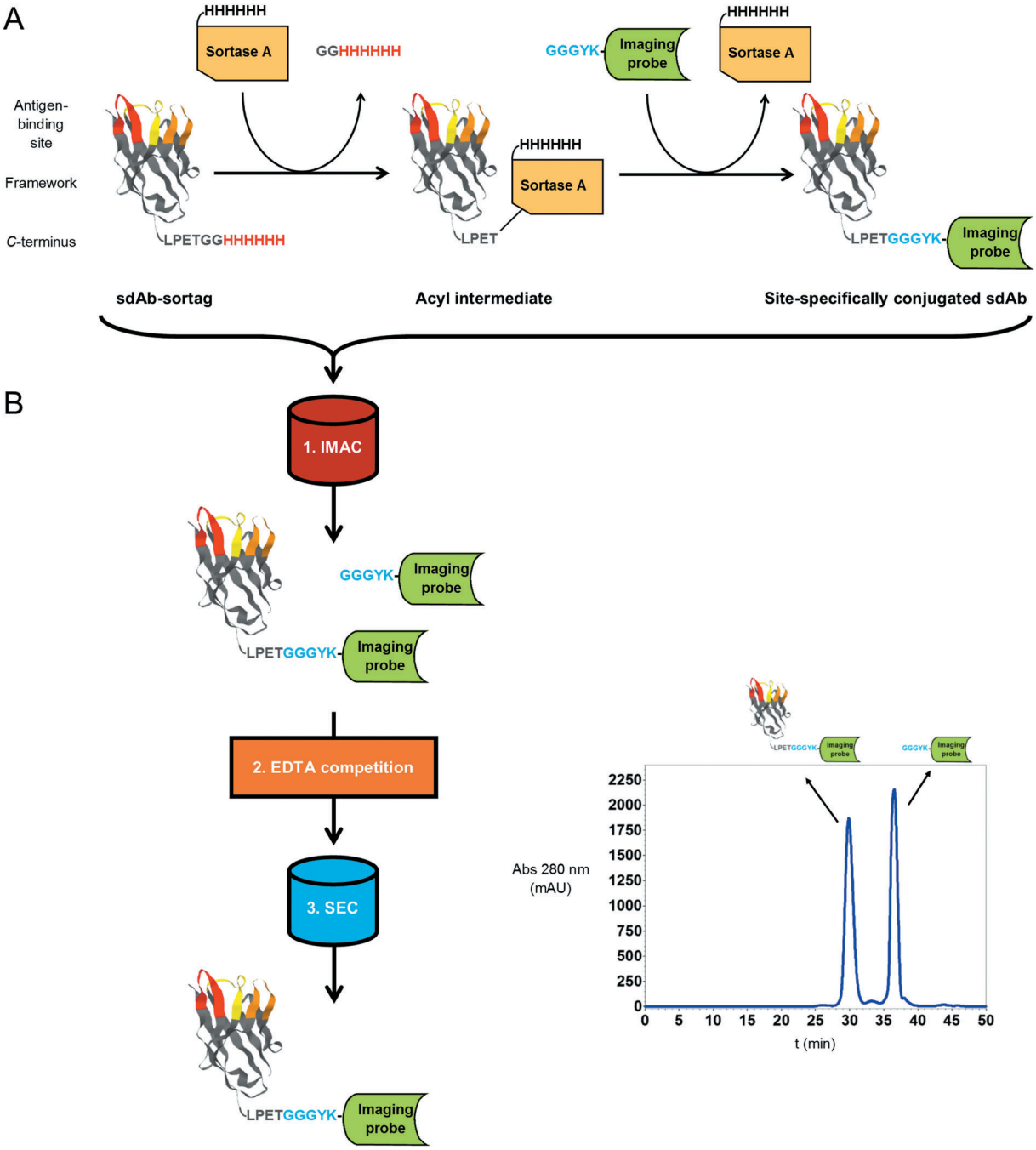

Figure 1. A) SrtA-mediated conjugation is a generic conjugation method. First, SrtA recognizes the *C*-terminal sortag of the sdAb and cleaves the peptide bond between T and G, with release of the downstream His-tag. Next, a nucleophilic attack of the triglycine-functionalized imaging probe on the acyl-enzyme intermediate leads to the formation of a new peptide bond with the sdAb, resulting in the site-specifically conjugated sdAb. B) Schematic overview of the purification strategy. After SrtA-mediated conjugation the reaction mixture contains, apart from the product-of-interest (conjugated sdAb), also unreacted sdAb, acyl-enzyme intermediate, imaging probe, SrtA and processed His-tags. Except for the imaging probe, all other undesired products contain a His-tag. This allows to capture all His-tagged products via IMAC with Ni-sepharose beads on an FPLC system in a first purification step. Next, the collected flow-through (composed of conjugated sdAb and imaging probe) is incubated with an excess of EDTA to remove Ca^{2+} ions, that were present as a cofactor of SrtA in the reaction buffer, and Ni^{2+} ions, that could leak from the Ni-sepharose beads, and prevent them from occupying the chelating agents. After sample volume reduction by concentration, the final purification step consisted of SEC on an FPLC system (inset, chromatogram for CHX-A"-DTPA-2Rs15d is shown) to separate the product-of-interest from the excess of nucleophilic imaging probe.

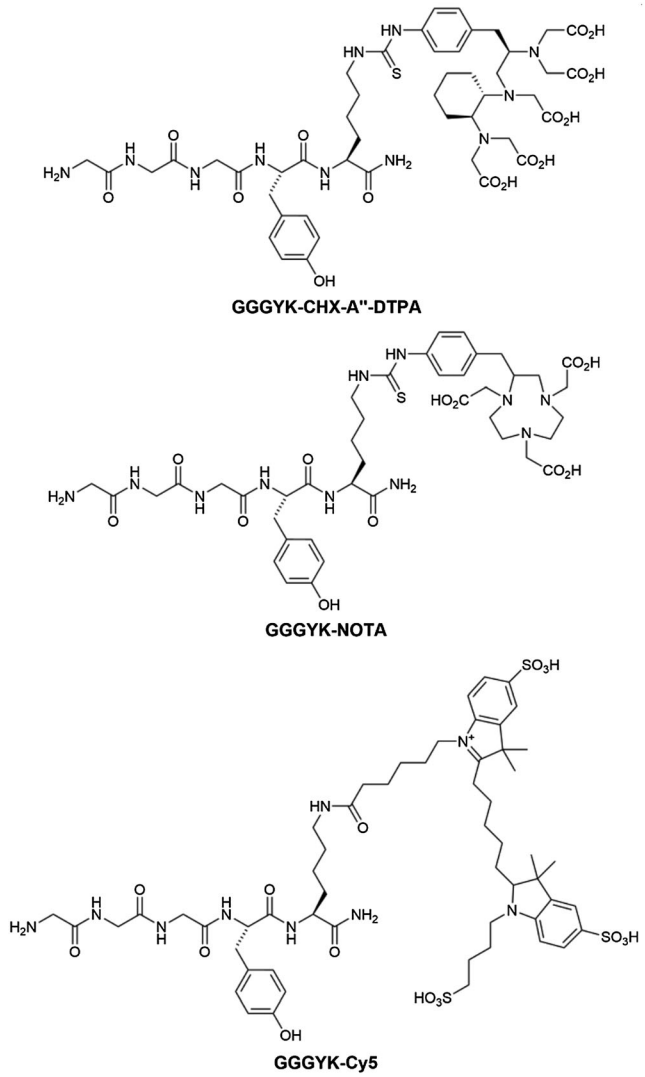

Figure 2. The imaging probes are composed of the pentapeptide H-GGGYK-NH_2 with the chelating agents CHX-A"-DTPA or NOTA, or the fluorescent dye Cy5, coupled to the ε-amine group of the lysine residue. The synthesis is described in supplementary material and methods.

the unreacted imaging probe (Fig. 1B). The deconvoluted mass spectra of the final purified products showed a homogeneous population of a single-conjugated imaging tracer (Fig. 4). The overall conversion yield of unconjugated to conjugated sdAb, taking into account both the reaction efficiency and purification procedure, was 48% ± 3% for sdAb 2Rs15d and 32% ± 4% for sdAb BcII10. For a given sdAb the yield did not differ significantly amongst the different nucleophilic imaging probes.

2.4. *In vitro* evaluation of the functionality after conjugation

The functionality of the sdAb-conjugates after SrtA-mediated conjugation was evaluated by surface plasmon resonance (SPR). The kinetic parameters of the antigen binding were determined on immobilized HER2 recombinant protein (Table 1). All three sdAb-conjugates CHX-A"-DTPA-2Rs15d, NOTA-2Rs15d and Cy5-2Rs15d conserved the same affinity for the HER2 antigen as the unconjugated starting product sdAb 2Rs15d-sortag. The kinetic characteristics of the latter were also not influenced by the addition of the sortag, in comparison to 2Rs15d-notag (the sdAb without any tag, previously used in a clinical PET-study) (16,17).

Furthermore, the fluorescence spectrum of sdAb Cy5-2Rs15d was compared to a reference sample of Cy5 dye without pentapeptide. To have the same dye concentrations, both samples were diluted to obtain equal absorbance at 650 nm (Fig. 5C). The spectrophotometric measurements showed that the fluorescence spectrum of the Cy5 dye was not negatively affected after SrtA-mediated conjugation.

2.5. Radiolabeling

CHX-A"-DTPA-conjugated sdAbs, at a concentration of 10 μM, were radiolabeled with ^{111}In ($t_{1/2}$ = 68 h) with activities ranging from 19 to 186 MBq. The obtained radiochemical purity was > 98% (Fig. 5A) and the variation in starting activity did not affect the labeling yield. Conversely, for radiolabeling with ^{68}Ga ($t_{1/2}$ = 68 min) the concentration of NOTA-conjugated sdAbs was 2 μM and it was incubated with activities ranging from 17 to 431 MBq, which resulted in a radiochemical purity of > 97% (Fig. 5B).

Prior to *in vivo* use the radiolabeled sdAbs were further purified by gel-filtration chromatography and filtration. The final radiochemical purity was > 99% and the decay-corrected radiochemical yield after purification was 79% ± 2% for ^{111}In-CHX-A"-DTPA-2Rs15d and 71% ± 4% for ^{68}Ga-NOTA-2Rs15d. The targeting capacity of the sdAbs after the radiolabeling procedures was evaluated in an *in vitro* cell binding study. sdAbs ^{111}In-CHX-A"-DTPA-2Rs15d and ^{68}Ga-NOTA-2Rs15d were still able to bind HER2-expressing BT474M1 cells specifically, and to the same extent as the lysine-conjugated variants (Fig. S2).

2.6. *In vivo* tumor targeting

Finally, the performance of the labeled sdAbs as imaging tracers was evaluated in an *in vivo* tumor-targeting experiment with BT474M1-xenografted mice. In each of the respective imaging modalities sdAbs ^{111}In-CHX-A"-DTPA-2Rs15d, ^{68}Ga-NOTA-2Rs15d and Cy5-2Rs15d were able to visualize the HER2-expressing tumor with high contrast already 1.0 h post-injection (Fig. 6 and S3, Movies S1 and S2). Besides the tumor also the kidneys and urinary bladder can be seen which is due to the typical excretion pattern of tracers with a molecular weight below the renal cut-off value of 60 kDa. The *ex vivo* biodistribution analyses at 1.5 h post-injection of the radiolabeled sdAbs confirmed these imaging results (Table 2). sdAbs ^{111}In-CHX-A"-DTPA-2Rs15d and ^{68}Ga-NOTA-2Rs15d targeted the tumor specifically compared to a non-targeting control sdAb BcII10 (12.00% ± 4.58% injected activity per gram of tissue (IA/g) vs. 1.07% ± 0.51% IA/g for ^{111}In-CHX-A"-DTPA-2Rs15d and ^{111}In-CHX-A"-DTPA-BcII10, respectively; and 14.07% ± 2.92% IA/g vs. 1.41% ± 1.13% IA/g for ^{68}Ga-NOTA-2Rs15d and ^{68}Ga-NOTA-BcII10, respectively). The uptake was low in all other non-targeted organs except for the kidneys. The fast blood clearance and tumor specificity are confirmed by the high tumor-to-blood and tumor-to-muscle ratios.

3. DISCUSSION

The site-specific labeling of targeting probes for diagnostic and therapeutic applications is of interest to obtain a well-defined homogeneous product with batch-to-batch consistency that

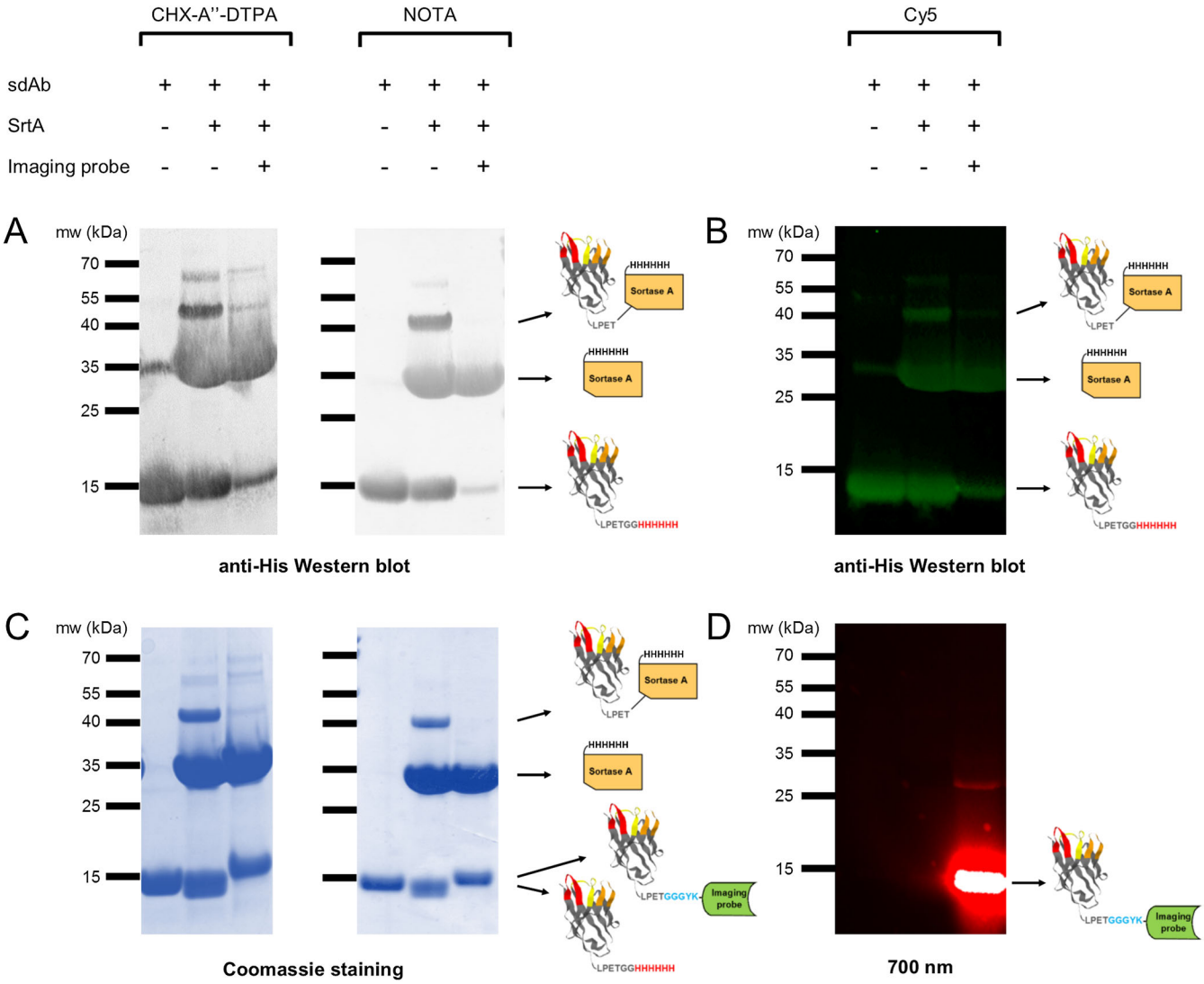

Figure 3. Determination of the reaction efficiency for conjugation of CHX-A"-DTPA (left), NOTA (middle) and Cy5 (right) to sdAb 2Rs15d. The contents of the reaction mixture were varied as indicated with + (present) and – (absent). The concentrations used were 50 μM sdAb 2Rs15d-sortag, 150 μM SrtA and 1.5 mM imaging probe. The reaction mixture was incubated overnight. The anti-His-tag Western blot (A and B) detects all His-tagged products in the reaction mixtures (unreacted sdAb, SrtA and acyl-enzyme intermediate). In the absence of imaging probe there was a clear accumulation of acyl-enzyme intermediate since the reaction could not proceed. When all three reaction components were present a high sdAb substrate consumption was obtained (≥ 75%), as shown by the weaker sdAb band compared to the control reaction that only contained sdAb substrate. The Coommassie staining of the corresponding LDS-PAGE (C) is shown as a control for the total amount of sdAb loaded, as both His-tagged and conjugated (without His-tag) sdAbs are visible. In the 700 nm fluorescence channel (D) the successful conjugation of Cy5 to sdAb 2Rs15d was visualized (saturated signal). The band with an apparent molecular weight between 55 and 70 kDa probably corresponds to a dimeric form of SrtA, which was reported before to be visible in reducing sodium dodecyl sulphate PAGE (15).

allows straightforward characterization and clinical translation. Here we explored SrtA-mediated conjugation as a generic approach for site-specific labeling of sdAbs.

The chemoenzymatic conjugation by SrtA requires the presence of the sortag LPXTG at the desired conjugation site in the substrate protein. Upon recognition of this peptide motif, the enzyme cleaves the peptide bond between the threonine and glycine residues, with loss of the downstream part of the substrate protein, and then forms a new peptide bond with the *N*-terminal glycine of a nucleophilic probe. In our approach the sortag LPETG was recombinantly introduced at the *C*-terminal end of the sdAb. The *C*-terminus is an ideal site for conjugation since it is located opposite to the antigen-binding site (18), hereby avoiding antigen-binding interference, and it renders the strategy generic. The inclusion of a His-tag downstream of the sortag allowed purification of the sdAb via IMAC during sdAb production, while it resulted in the loss of the His-tag upon conjugation. The latter is a great advantage for clinical translation where the use of His-tagged proteins is avoided since they increase the possible risk of immune responses (19). Of note, the safety profile of the use of SrtA-mediated conjugation in clinical tracer production, and in particular the non-immunogenic character of the sortag and absence of metal contaminants coming from the IMAC step in purification, still needs to be verified.

Another important aspect for a generic labeling method is the flexibility of SrtA towards its nucleophilic substrates. Antibodies and antibody-derived fragments have already been functionalized with fluorescent labels for *in vitro* detection (20,21), as well

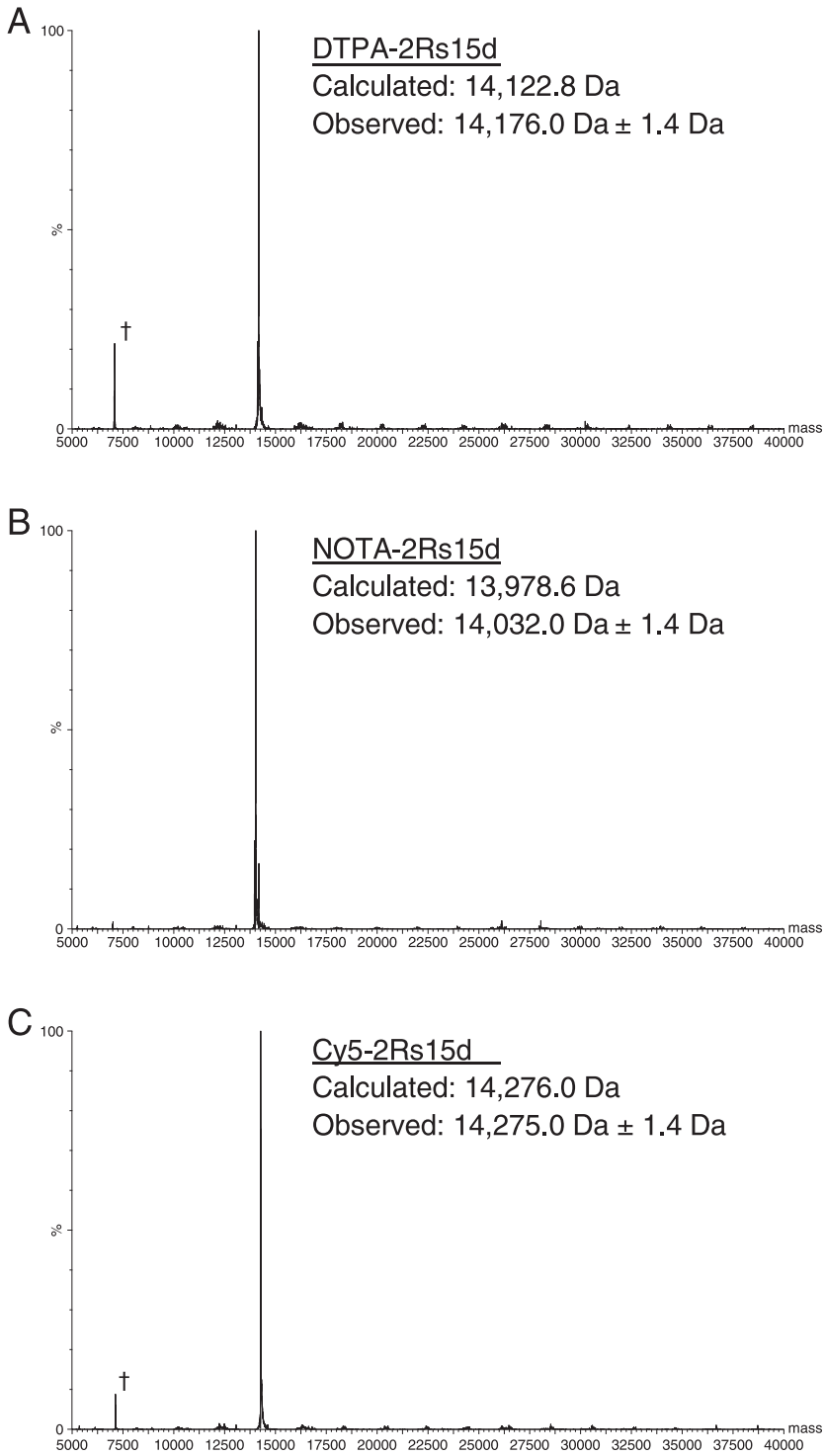

Figure 4. The purified sdAb-conjugates CHX-A"-DTPA-2Rs15d (A), NOTA-2Rs15d (B) and Cy5-2Rs15d (C) are homogeneous single-conjugated sdAbs. Unreacted sdAb (14,430.0 Da), SrtA (22,133.9 Da) and the acyl-enzyme intermediate (35,182.5 Da) are absent in the ESI-Q-ToF deconvoluted mass spectra. In (A) and (B), complexation of Fe by the chelating agents is seen (net change in calculated mass of + 52.8 Da). However, this did not interfere with further radiolabeling. (†: Peak arising from artifact in deconvolution)

as with toxins and polymeric capsules for targeted drug delivery (22–24). The feasibility of installing bioorthognal click chemistry handles gave rise to even more opportunities, including the generation of *C*-terminus-to-*C*-terminus sdAb dimers (25) and the oriented immobilization on nanosheets (26), without sterical hindrance of the antigen-binding regions upon dimerization or immobilization. Not surprisingly, SrtA-mediated conjugation also found its way into the field of *in vivo* molecular imaging. So far it was employed for the functionalization of scFv's (single-chain variable fragment) and sdAbs with iron oxide particles for use in magnetic resonance imaging (MRI) (27), microbubbles for ultrasound imaging (28) and the radiolabels ^{64}Cu and ^{18}F for PET

Table 1. The kinetic parameters of sdAb 2Rs15d are preserved after SrtA-mediated conjugation with CHX-A"-DTPA, NOTA or Cy5

	k_a 10^5 M^{-1} s^{-1}	k_d 10^{-4} s^{-1}	K_D 10^{-9} M	Chi^2 RU^2
2Rs15d-notag	1.8	7.0	3.8	0.07
2Rs15d-sortag	1.5	5.1	3.4	0.11
CHX-A"-DTPA-2Rs15d	1.5	5.4	3.7	0.16
NOTA-2Rs15d	1.4	5.3	3.7	0.09
Cy5-2Rs15d	1.5	6.1	4.1	0.14

SPR measurements are performed on immobilized HER2 recombinant protein. The kinetic parameters of 2Rs15d-notag (the sdAb without any tag) (16) and 2Rs15d-sortag are given as a reference.
(k_a, association reaction rate constant; k_d, dissociation reaction rate constant; K_D, dissociation equilibrium constant; RU, resonance units; all values had SE < 0.1)

(29–32). Here we applied SrtA-mediated conjugation for the site-specific labeling of sdAbs with ^{111}In, ^{68}Ga and Cy5 to produce imaging tracers for SPECT, PET and FRI, respectively. Together with the aforementioned reports this demonstrates the versatility and efficacy of SrtA to produce imaging tracers for multiple non-invasive *in vivo* imaging modalities.

The pentapeptide H-GGGYK-NH_2 formed the base of the imaging probes. It contained an *N*-terminal triglycine to fulfill the nucleophilic attack in the chemoenzymatic reaction and a lysine residue for side chain conjugation of the chelating agents CHX-A"-DTPA-NCS or NOTA-NCS, or the fluorescent dye Cy5. We preferred the employment of the side chain ε-amine of lysine as the acceptor for carboxylated chelating agents and fluorescent dyes, over the side chain sulfhydryl of cysteine as acceptor for maleimide-functionalized probes, to avoid the introduction of a potentially reversible thioether succinimide linkage (33,34). This thioether succinimide linkage probably does not affect diagnostic imaging with low molecular weight imaging tracers at early time points after injection, but should certainly be avoided for targeted radionuclide therapy with longer-lived isotopes.

After optimization of the substrate concentrations and incubation time, the conjugation was carried out in an overnight reaction with a threefold molar excess of SrtA and a thirtyfold molar excess of imaging probe, relative to the sdAb concentration, and resulted in a sdAb substrate consumption above 75%. These results were obtained with the solubilized form of the wild type SrtA from *S. aureus* (35). However, the use of a mutant form of SrtA with an improved catalytic activity could still increase this reaction efficiency and would allow to lower product consumption (36). After the purification of the conjugated sdAb the overall efficiency of the procedure was 30 to 50%, meaning that a reaction starting with 1.0 mole of sdAb yields 0.3 to 0.5 mole of purified, conjugated product. Mass spectrometry analysis of the conjugated sdAbs confirmed that only one chelating agent or fluorescent dye was attached, and did not detect the presence of any unreacted substrate or side-product. For CHX-A"-DTPA- and NOTA-conjugated sdAbs complexation with Fe was detected, probably arising from Fe contamination in the buffers used for conjugation. Contrary to the radiolabeling buffers, the conjugation reaction buffer was not treated against metal

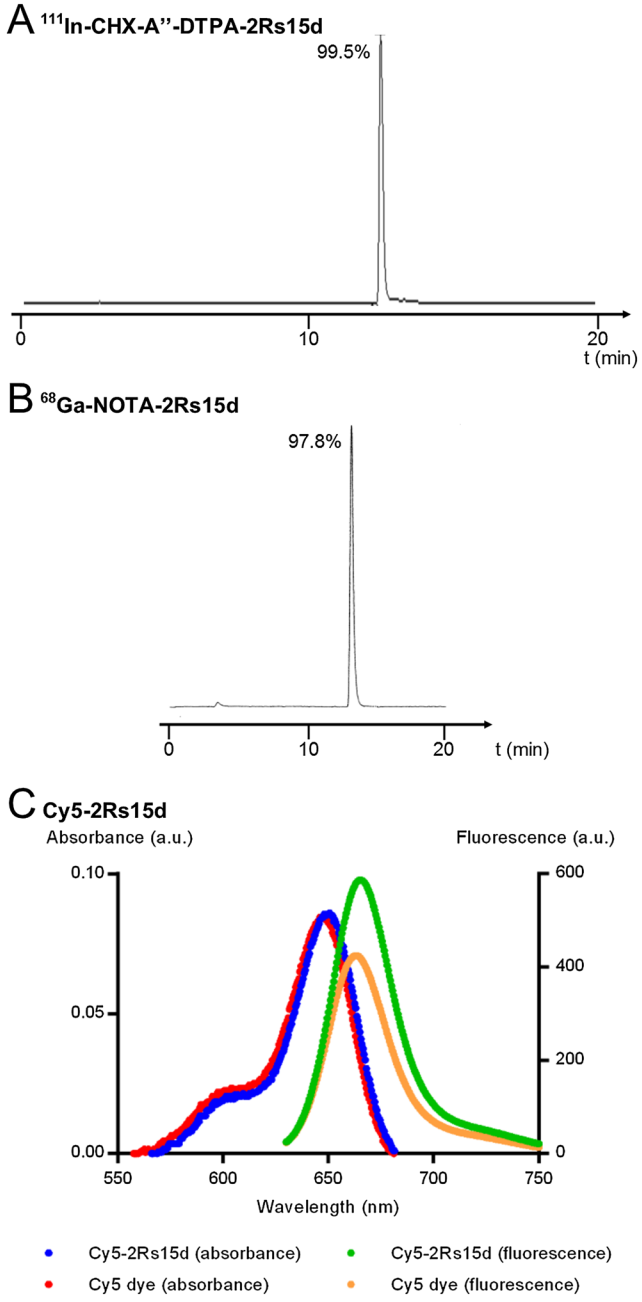

Figure 5. SrtA-mediated conjugation does not interfere with radiolabeling or the spectral characteristic of the fluorescent dye. RP-HPLC analysis of ^{111}In-CHX-A"-DTPA-2Rs15d (A) and ^{68}Ga-NOTA-2Rs15d (B) showed a high radiochemical purity after radiolabeling. The γ-spectrum chromatogram of a representative experiment is shown (3 min: free ^{111}In or ^{68}Ga; 13 min: radiolabeled sdAb). C) Spectrophotometric characterization of sdAb Cy5-2Rs15d compared to unconjugated Cy5 dye (without pentapeptide) as a standard. For two samples having the same dye concentration (equal absorbance spectra), the increased intensity of the fluorescence spectrum of Cy5-2Rs15d showed that the Cy5 dye is not stacked after conjugation to sdAb 2Rs15d.

contamination since this would interfere with the Ca^{2+} concentration, a necessary cofactor of SrtA. An alternative could be to use a Ca^{2+}-independent form of SrtA derived from another bacterial strain (e.g. *Streptococcus pyogenes*) (37) or by mutation of the SrtA from *S. aureus* (38). Nevertheless, the Fe-contamination did not interfere with radiolabeling as high radiochemical

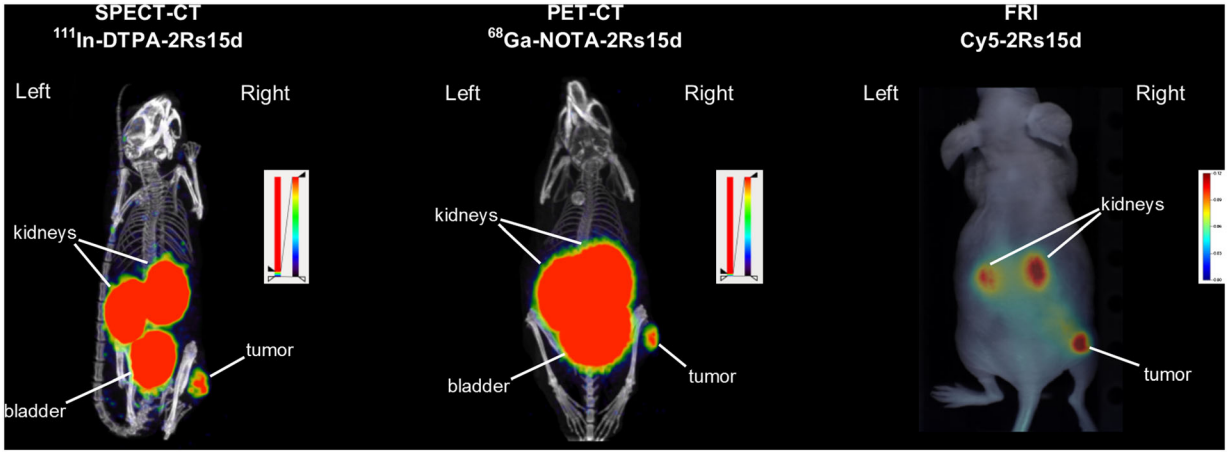

Figure 6. sdAb 2Rs15d targets HER2-positive BT474M1 tumors in mice, leading to high contrast in multiple imaging modalities, already at 1.0 h post-injection. Maximum-intensity-projections are shown for SPECT-CT and PET-CT, 2D dorsal view is shown for FRI.

Table 2. sdAbs ^{111}In-CHX-A"-DTPA-2Rs15d and ^{68}Ga-NOTA-2Rs15d show a significant tumor uptake in HER2-expressing BT474M1-xenografts compared to non-targeting control sdAbs, with low uptake in all other non-targeted organs except kidneys (renal excretion)

	^{111}In-CHX-A"-DTPA-2Rs15d	^{111}In-CHX-A"-DTPA-BcII10	^{68}Ga-NOTA-2Rs15d	^{68}Ga-NOTA-BcII10
Blood	0.46 ± 0.23	0.61 ± 0.25	0.41 ± 0.07	0.29 ± 0.15
Heart	0.21 ± 0.06	0.29 ± 0.09	0.21 ± 0.04	0.18 ± 0.10
Lungs	0.46 ± 0.16	0.72 ± 0.22	0.92 ± 0.25	0.71 ± 0.08
Liver	0.33 ± 0.08	0.37 ± 0.12	0.32 ± 0.18	0.35 ± 0.05
Spleen	0.16 ± 0.04	0.19 ± 0.07	0.24 ± 0.06	0.17 ± 0.08
Pancreas	0.12 ± 0.03	0.16 ± 0.05	0.16 ± 0.04	0.11 ± 0.05
GI tract†	0.68 ± 0.26	0.76 ± 0.06	1.07 ± 0.53	0.66 ± 0.14
Kidney	117.99 ± 5.13 *	213.84 ± 10.26	124.68 ± 13.92	137.40 ± 34.32
Muscle	0.62 ± 0.68	0.29 ± 0.14	0.26 ± 0.05	0.28 ± 0.06
Bone	0.36 ± 0.37	0.25 ± 0.05	0.31 ± 0.07	0.48 ± 0.53
Tumor	12.00 ± 4.58 *	1.07 ± 0.51	14.07 ± 2.92 *	1.41 ± 1.13
Tumor-to-Blood	31.19 ± 15.84 *	1.94 ± 0.96	34.50 ± 4.24 *	6.33 ± 6.57
Tumor-to-Muscle	30.70 ± 21.01 *	4.01 ± 1.61	55.58 ± 8.63 *	5.20 ± 4.45

The biodistribution profile was determined *ex vivo* at 1.5 h post-injection and is expressed as % IA/g ± SD.
(GI tract, gastrointestinal tract)
†: % IA is given
*: $p < 0.01$ compared to the non-targeting control sdAb BcII10; n = 5–6

purities (>97%) were obtained at the end of the radiolabeling reactions.

The SrtA-mediated labeling strategy was set up and validated in a HER2-positive xenografted cancer model. HER2 is a type 1 transmembrane receptor which is overexpressed in approximately 20% of breast cancer patients and is associated with low overall survival (39). Therefore the development of personalized anti-HER2 therapeutic strategies and methods for identification of patients that would benefit from those therapies is of utmost interest. Previously sdAb 2Rs15d, which was developed against HER2, has shown preclinically to be an excellent targeting agent for such purposes (16,40,41), and a PET-CT protocol with ^{68}Ga-$(NOTA)_{1.5}$-2Rs15d was recently found safe in a clinical phase 1 study (17). Initial characterization of the anti-HER2 binders and the selection of a lead compound was done with ^{99m}Tc-labeled sdAbs (41). Although it is a convenient and site-specific labeling method for preclinical screening of His-tagged sdAbs (42), ^{99m}Tc-tricarbonyl chemistry has a rather limited applicability in a context of multiple imaging modalities. Alternatively, sdAb 2Rs15d was randomly conjugated on lysine residues without loss of targeting efficacy (16), which was confirmed in a direct comparison between randomly and site-specifically conjugated sdAbs in the *in vitro* cell binding assay in this study and in previous work (5). Of note, the sdAb 2Rs15d was originally selected because of the absence of lysine residues in the antigen-binding region. Such criterion is however a big burden, as for example in the case of our anti-HER2 sdAbs where it excluded seven out of the seventeen identified families (unpublished data from Vaneycken *et al.*) (41). The availability of a generic site-specific labeling method via a *C*-terminal sortag omits the need for such an exclusion criterion in future lead compound selections.

Here we employed SrtA-mediated conjugation for the site-specific labeling of sdAb 2Rs15d with ^{111}In, ^{68}Ga and Cy5. In the three corresponding imaging modalities SPECT-CT, PET-CT and FRI, respectively, the 2Rs15d-conjugates were able to visualize the HER2-positive tumor in BT474M1 xenografts with high contrast as early as 1 h post-injection. The *ex vivo* biodistribution analysis of ^{111}In-CHX-A"-DTPA-2Rs15d and ^{68}Ga-NOTA-2Rs15d confirmed the conservation of the targeting efficiency after SrtA-mediated conjugation, with a high and specific tumor uptake at 90 min post-injection and low background in all other non-targeted organs, except kidneys. The difference in kidney retention between ^{111}In-CHX-A"-DTPA-2Rs15d and ^{111}In-CHX-A"-DTPA-BcII10 can be partially attributed to the difference in sdAb protein sequence. However, the ^{68}Ga labeled compound does not show such a profound difference, so the influence of the chelating agent and radiolabel should not be neglected. Furthermore ^{68}Ga-NOTA-2Rs15d showed a higher kidney uptake compared to the lysine conjugated ^{68}Ga-$(NOTA)_{1.5}$-2Rs15d (16), while both sdAb derivatives lack a His-tag. This indicates the possible influence of the applied conjugation method on kidney retention during tracer elimination and should be investigated further. Also, the use of SrtA-mediated labeling can be further explored for targeted radionuclide therapy by radiolabeling of the chelating agent CHX-A"-DTPA with ^{177}Lu (43), or by conjugating other chelating agents or functional groups to the pentapeptide of the nucleophlic probe.

4. CONCLUSION

We presented a detailed SrtA-mediated site-specific labeling approach of sdAbs for subsequent application in non-invasive *in vivo* molecular imaging. This labeling strategy resulted in a homogeneous, site-specifically single-conjugated tracer with uncompromised functionality. We illustrated its versatility by conjugating three different imaging probes for three different *in vivo* imaging modalities. The introduction of the sortag at the *C*-terminal end of the sdAb makes this strategy a generic approach for a wide range of future site-specific labelings of sdAbs.

5. EXPERIMENTAL

5.1. Recloning, expression and production of sdAbs

The generation and biochemical characterization of the anti-HER2 sdAb 2Rs15d and the non-targeting control sdAb BcII10 (developed against bacterial beta-lactamase) have been described previously (41,44). The NcoI – BstEII digested PCR fragment, encoding the sdAb region, was ligated in-frame into the pHEN29 plasmid, cut with the same restriction enzymes. The pHEN29 expression vector is derived from the pHEN6 vector, an *Escherichia coli* expression plasmid containing the pelB signal sequence to translocate the recombinant protein with a *C*-terminal His-tag to the periplasm (44). In the pHEN29 expression vector, the sortag LPETG codons are inserted between the sdAb and His-tag codons, which are followed by the EPEA codons for an E-tag (Fig. S4).

The sdAbs were produced in bacteria containing the pHEN29 recombinant expression plasmid and purified from the periplasm by IMAC and SEC, as described in detail elsewhere (45). In short, sdAbs were translocated to the periplasm of *E. coli* WK6 cells, from which they were collected with an osmotic shock. sdAbs were purified from the periplasmic extract via IMAC with HIS-select suspension (Sigma-Aldrich, Saint Louis, MO, USA) and subsequent SEC on a HiLoad 16/600 Superdex 75 PG column (GE Healthcare, Uppsala, Sweden) equilibrated in PBS (pH 7.4).

The sdAb concentrations were determined spectrophotometrically at 280 nm using the theoretically calculated extinction coefficient (46).

An *in silico* predicted structure of sdAb 2Rs15d was generated using ESyPred3D (47).

5.2. SrtA-mediated conjugation

Prior to SrtA-mediated conjugation the buffer of the sdAbs was changed to 50 mM Tris-HCl (pH 7.9), 150 mM NaCl using a Vivaspin 2 concentrator (MWCO 5000) (Sartorius) according to the manufacturer's protocol. The lyophilized nucleophilic probes were dissolved in 50 mM Tris-HCl (pH 7.9), 150 mM NaCl as a 10 mM stock solution.

For optimization of the conjugation reaction, small-scale reactions were set up in 40 μL with variable concentrations of SrtA and nucleophilic probe and variable incubation times.

The most optimal conditions were upscaled to a volume of 1.5 mL. The reaction mixture was composed of 50 μM sdAb, 150 μM SrtA and 1.5 mM nucleophilic probe, with 50 mM Tris-HCl (pH 7.9), 150 mM NaCl, 10 mM $CaCl_2$ as the reaction buffer. The reaction was allowed to take place overnight at 37 °C.

5.3. Reducing lithium dodecyl sulphate polyacrylamide gel electrophoresis (LDS-PAGE) and Western blot

Samples from overnight reaction mixtures containing 5 μg sdAb were mixed with NUPAGE LDS sample buffer and NUPAGE sample reducing agent (Life technologies, Carlsbad, CA, USA) according to the manufacturer's protocol. After incubation at 70 °C for 10 min, samples were run on a NUPAGE 12% Bis-Tris gel (Life technologies) in MES buffer. PageRuler prestained protein ladder (Thermo Fisher Scientific, Rockford, IL, USA) was used as molecular weight marker. When complete separation was obtained the gel was stained with Coomassie Brilliant Blue for total protein visualization or further processed in Western blot to reveal His-tagged products. For the latter, proteins were transferred from the LDS polyacrylamide gel to a 0.45 μm nitrocellulose membrane (GE Healthcare). The residual protein binding sites on the membrane were subsequently blocked by incubation in PBS (pH 7.4) supplemented with milk powder (2%) for 2 h at 4 °C. His-tagged products were detected by using mouse anti-histidine tag (AbD Serotec, Oxford, UK) as the primary antibody and goat anti-mouse IgG peroxidase conjugate (Sigma-Aldrich) (only for CHX-A"-DTPA and NOTA conjugates) or goat anti-mouse IgG-IrDye800CW (LI-COR) as the secondary antibody, with thorough washing with PBS-Tween (0.05%) (pH 7.4) in between. Western blots where the peroxidase-conjugated detection antibody was used, were developed using 4-chloro-1-napthol (Sigma-Aldrich). The IrDye800CW-conjugated detection antibody was visualized using an Odyssey imaging scanner (LI-COR, Lincoln, NE, USA) at 800 nm.

Intensities of the sdAb bands were determined by measuring the integrated intensities in the 800 nm-channel with the Odyssey imaging software (LI-COR).

5.4. Purification of the conjugated sdAbs

In the first step of the purification procedure all His-tagged products were captured from the reaction mixture via IMAC, using a

1 mL HisTrap HP column (GE Healthcare). The purification was done in three runs (injection of 500 μL reaction mixture per run) with 50 mM Tris-HCl (pH 7.9), 150 mM NaCl as running buffer at a flow rate of 0.3 mL/min. The flow-through was collected based on its absorption of UV light at 280 nm. Subsequently the collected flow-through was incubated with 15 mM EDTA (final concentration) for 30 min at 37 °C. Prior to SEC purification, the sample's volume was reduced using a Vivaspin 2 device (MWCO 5000) (Sartorius, Goettingen, Germany) according to the manufacturer's protocol. The SEC purification was performed on a Superdex 75 10/300 GL column (GE Healthcare) at a flow rate of 0.5 mL/min with elution in 0.1 M NH_4OAc (pH 7.0) (treated with Chelex-100 (Sigma-Aldrich)) for CHX-A"-DTPA- and NOTA-conjugated sdAbs, and in PBS (pH 7.4) for Cy5-conjugated sdAbs. The overall yield was determined by comparison of the moles of purified conjugate to the moles of sdAb used to start the reaction.

5.5. Electrospray ionization quadrupole time-of-flight (ESI-Q-ToF) mass spectrometry of purified sdAb-conjugates

Samples were desalted using an Amicon device (MWCO 3000) (Merck Millipore, Darmstadt, Germany) according to the manufacturer's protocol and placed in 25 mM NH_4OAc buffer. The samples were analyzed on an ESI-Q-ToF (Waters, Milford, MA, USA) in positive ion mode at an estimated protein concentration of 10 μM in 25 mM NH_4OAc, 30% acetonitrile, 0.5% formic acid. Spectra deconvolution technique was the maximum entropy Max ent1. Theoretical masses were calculated using ChemBioDraw Ultra 14.0 (PerkinElmer, Waltham, MA, USA).

5.6. SPR

The kinetic parameters of antigen binding by sdAb 2Rs15d and sdAb-conjugates were determined via SPR with a Biacore T200 (GE Healthcare). The HER2-Fc recombinant fusion protein (Sino Biologicals, Beijing, China) was immobilized in 10 mM sodium acetate (pH 4.5) on a CM5 chip (GE Healthcare) via amine coupling chemistry to 740 response units. sdAbs were analysed in a two-fold serial dilution (125 nM – 0.488 nM) in HBS with an analyte flow rate of 10 μL/min. The association phase took 180 s and the dissociation phase 600 s. Binding curves were fitted using a '1:1 (antigen:analyte) with drift and RI2' binding model in Biacore T200 evaluation software.

5.7. UV-VIS and fluorescence spectrophotometric measurements of Cy5-conjugated sdAb

A sample of Cy5-2Rs15d was prepared in H_2O in a 3.0 mL quartz cuvette, reaching an absorbance below 0.1 at 650 nm (approximately 0.3 μM). Then a sample of the unconjugated Cy5 dye (without pentapeptide) was prepared with the same absorbance at 650 nm. Both samples were measured with an Ultrospec3000 UV-VIS spectrophotometer (Amersham Pharmacia Biotech, Piscataway, NJ, USA). The fluorescent output of both samples was measured with a LS55 fluorescence spectrometer (Perkin Elmer). The samples were excited at 650 nm and emission light was measured between 630 and 750 nm, with the excitation slit at 10 nm and the emission slit at 7 nm.

5.8. Radiolabeling procedures

Buffers used for radiolabeling were purified from metal contaminants with Chelex-100 (Sigma-Aldrich).

CHX-A"-DTPA-conjugated sdAbs were radiolabeled with $InCl_3$ (Mallinckrodt Pharmaceuticals) (19 to 186 MBq) at a final sdAb concentration of 10 μM in reaction volumes of 100 to 500 μL with 0.2 M NH_4OAc buffer (pH 5.0). After incubation for 30 min at 50 °C, the radiochemical purity was determined via instant thin-layer chromatography (iTLC) on silica gel (Pall Corporation, Port Washington, NY, USA) with 0.1 M sodium citrate (pH 5.0) as eluent.

^{68}Ga was eluted in 0.1 N HCl from a $^{68}Ge/^{68}Ga$ generator (Eckert & Ziegler, Berlin, Germany). NOTA-conjugated sdAbs were diluted in 0.1 to 1.0 mL sodium acetate (0.1 M, pH 5.0) and mixed with an equal volume of the ^{68}Ga-eluate (17 to 431 MBq), to obtain a final sdAb concentration of 2 μM. After incubation for 10 min at 37 °C, the radiochemical purity was determined via iTLC as described above.

Prior to *in vivo* use the radiolabeled tracers were purified via gel-filtration chromatography on Illustra NAP-5 or PD-10 desalting columns (both from GE Healthcare), for ^{111}In- and ^{68}Ga-radiolabeled tracers, respectively, with elution in PBS-Tween (0.1%) (pH 7.4) according to the manufacturer's protocol. Finally, they were passed through a 0.22 μm PVDF membrane filter (Merck Millipore).

5.9. RP-HPLC

RP-HPLC analysis of the radiolabeled sdAbs was performed on a polystyrene divinylbenzene copolymer column (PLRP-S 300 Å, 5 μm, 250/4 mm; Varian, Santa Clara, CA, USA). The following gradient was used (A: H_2O, 0.1% trifluoroacetic acid; B: acetonitrile, 0.1% trifuoroacetic acid): 0 – 5 min, 75%A/25% B; 5 – 7 min, 75%A/25%B – 66%A/34% B; 7 – 10 min, 66%A/34%B – 100% B; 10–20 min, 100% B; at a flow rate of 1 mL/min.

5.10. Animal models

All animal study protocols were approved by the Ethical committee for animal experiments of the Vrije Universiteit Brussel. All manipulations were done under the control of 2.5% isoflurane (Abbott, Abbott Park, IL, USA). Female athymic nude mice (Charles River, Sulzfeld, Germany) received an estrogen pellet (0.36 mg 17β-estradiol, 60-day release) (Innovative Research of America, Sarasota, FL, USA) that was placed subcutaneously in the neck region. The next day the mice were inoculated subcutaneously in the right hind leg with $5x10^6$ BT474M1 cells in 100 μL growth medium (cell culturing conditions in supplementary material and methods), mixed with 100 μL Matrigel basement membrane matrix (Corning, Tewksbury, MA, USA). Tumors were grown for 4 weeks. Tumor sizes ranged from 20 to 335 mm^3.

5.11. *In vivo* imaging and *ex vivo* biodistribution analysis of radiolabeled tracers

BT474M1-xenografted mice (n = 5-6) were intravenously injected under the control of 2.5% isoflurane (Abbott). For SPECT-CT (single-photon emission computed tomography – X-ray computed tomography) acquisition and subsequent *ex vivo* biodistribution analysis they were administered 16 MBq of ^{111}In-CHX-A"-DTPA-2Rs15d (31 MBq/nmol) or ^{111}In-CHX-A"-DTPA-BcII10 (38 MBq/nmol). For *ex vivo* biodistribution analysis of the ^{68}Ga-labeled compounds they received 5 MBq of ^{68}Ga-NOTA-2Rs15d (21 MBq/nmol) or ^{68}Ga-NOTA-BcII10 (19 MBq/nmol). For PET-CT (positron emission tomography – X-ray computed tomography) acquisition the administered dose was increased (11 MBq, 37 MBq/nmol).

SPECT-CT and PET-CT acquisition and reconstruction details are described in supplementary material and methods. Images were analysed using OsiriX (Pixmeo, Bernex, Switzerland).

Animals were dissected at 1.5 h post-injection. Organ activities were measured against a standard of known activity with a gamma counter (Cobra II inspector 5003, Canberra-Packard, Downers Grove, IL, USA) and expressed as % IA/g, corrected for decay and paravenous activity in the tail.

5.12. *In vivo* imaging analysis of Cy5-labeled tracers

BT474M1-xenografts (n = 3), fed on a low-fluorescent diet (2016 Teklad Global 16% Protein Rodent Diet, Harlan, Indianapolis, IN, USA), were intravenously injected under the control of 2.5% isoflurane (Abbott) with 2 nmol of Cy5-2Rs15d or Cy5-BcII10.

At 1.0 h post-injection, animals were anesthetized with 2.5% isoflurane (Abbott) and positioned in a fluorescence imaging system (FMT2500, PerkinElmer). Reflectance images of the dorsal and ventral side of the animals were acquired in the 635 nm channel. Images were analyzed using TrueQuant (PerkinElmer).

5.13. Statistical analysis

The statistical analysis was performed in SPSS Statistics 22 (IBM, Chicago, IL, USA). *Ex vivo* biodistribution data were analysed using a nonparametric Mann-Whitney U test for two independent samples.

Acknowledgements

The authors thank Cindy Peleman, Christian Bartz and Santina Gorsen for experimental support, and Michel Defrise for support with the SPECT-CT reconstructions. Sam Massa and Tony Lahoutte are supported by the Research Foundation – Flanders (FWO) (PhD fellow and Senior clinical investigator, respectively). Christian Vanhove is supported by the GROUP-ID consortium of Ghent University. This work is funded by the Research Foundation – Flanders (FWO) (grant G066615N) and Strategic Research Program – Growth Funding of Vrije Universiteit Brussel. SrtA-encoding plasmid was kindly provided by Hidde Ploegh (Whitehead Institute for Biomedical Research, Cambridge, MA, USA). Cell line BT474M1 was kindly provided by Michael Zalutsky (Duke University Medical Center, Durham, NC, USA).

REFERENCES

1. Wang LT, Amphlett G, Blattler WA, Lambert JM, Zhang W. Structural characterization of the maytansinoid - monoclonal antibody immunoconjugate, huN901-DM1, by mass spectrometry. Protein Sci 2005; 14: 2436–2446. doi:10.1110/ps.051478705.
2. Alt K, Paterson BM, Ardipradja K, Schieber C, Buncic G, Lim B, Poniger SS, Jakoby B, Wang XW, O'Keefe GJ, Tochon-Dansuy HJ, Scott AM, Ackermann U, Peter K, Donnelly PS, Hagemeyer CE. Single-chain antibody conjugated to a cage amine chelator and labeled with positron-emitting copper-64 for diagnostic imaging of activated platelets. Mol Pharm 2014; 11: 2855–2863. doi:10.1021/mp500209a.
3. Kijanka M, Warnders FJ, El Khattabi M, Lub-de Hooge M, van Dam GM, Ntziachristos V, de Vries L, Oliveira S, van Bergen En Henegouwen PM. Rapid optical imaging of human breast tumour xenografts using anti-HER2 VHHs site-directly conjugated to IRDye 800CW for image-guided surgery. Eur J Nucl Med Mol Imaging 2013; 40: 1718–1729. doi:10.1007/s00259-013-2471-2.
4. Junutula JR, Raab H, Clark S, Bhakta S, Leipold DD, Weir S, Chen Y, Simpson M, Tsai SP, Dennis MS, Lu YM, Meng YG, Ng C, Yang JH, Lee CC, Duenas E, Gorrell J, Katta V, Kim A, McDorman K, Flagella K, Venook R, Ross S, Spencer SD, Wong WL, Lowman HB, Vandlen R, Sliwkowski MX, Scheller RH, Polakis P, Mallet W. Site-specific conjugation of a cytotoxic drug to an antibody improves the therapeutic index. Nat Biotechnol 2008; 26: 925–932. doi:10.1038/nbt.1480.
5. Massa S, Xavier C, De Vos J, Caveliers V, Lahoutte T, Muyldermans S, Devoogdt N. Site-specific labeling of cysteine-tagged camelid single-domain antibody-fragments for use in molecular imaging. Bioconjug Chem 2014; 25: 979–988. doi:10.1021/bc500111t.
6. Agarwal P, Bertozzi CR. Site-specific antibody–drug conjugates: the nexus of bioorthogonal chemistry, protein engineering, and drug development. Bioconjug Chem 2015; 26: 176–192. doi:10.1021/bc5004982.
7. Mazmanian SK, Liu G, Hung TT, Schneewind O. Staphylococcus aureus sortase, an enzyme that anchors surface proteins to the cell wall. Science 1999; 285: 760–763. doi:10.1126/science.285.5428.760.
8. Popp MWL, Ploegh HL. Making and breaking peptide bonds: protein engineering using sortase. Angew Chem Int Ed 2011; 50: 5024–5032. doi:10.1002/anie.201008267.
9. Schmohl L, Schwarzer D. Sortase-mediated ligations for the site-specific modification of proteins. Curr Opin Chem Biol 2014; 22C: 122–128. doi:10.1016/j.cbpa.2014.09.020.
10. Ritzefeld M. Sortagging: a robust and efficient chemoenzymatic ligation strategy. Chem Eur J 2014; 20: 8516–8529. doi:10.1002/chem.201402072.
11. Hamers-Casterman C, Atarhouch T, Muyldermans S, Robinson G, Hamers C, Songa EB, Bendahman N, Hamers R. Naturally-occuring antibodies devoid of light-chains. Nature 1993; 363: 446–448. doi:10.1038/363446a0.
12. De Vos J, Devoogdt N, Lahoutte T, Muyldermans S. Camelid single-domain antibody-fragment engineering for (pre)clinical *in vivo* molecular imaging applications: adjusting the bullet to its target. Expert Opin Biol Ther 2013; 13: 1149–1160. doi:10.1517/14712598.2013.800478.
13. Chakravarty R, Goel S, Cai WB. Nanobody: The 'magic bullet' for molecular imaging?. Theranostics 2014; 4: 386–398. doi:10.7150/thno.8006.
14. D'Huyvetter M, Xavier C, Caveliers V, Lahoutte T, Muyldermans S, Devoogdt N. Radiolabeled nanobodies as theranostic tools in targeted radionuclide therapy of cancer. Expert Opin Drug Del 2014; 11: 1939–1954. doi:10.1517/17425247.2014.941803.
15. Lu C, Zhu J, Wang Y, Umeda A, Cowmeadow RB, Lai E, Moreno GN, Person MD, Zhang Z. Staphylococcus aureus sortase a exists as a dimeric protein *in vitro*. Biochemistry 2007; 46: 9346–9354. doi:10.1021/bi700519w.
16. Xavier C, Vaneycken I, D'Huyvetter M, Heemskerk J, Keyaerts M, Vincke C, Devoogdt N, Muyldermans S, Lahoutte T, Caveliers V. Synthesis, preclinical validation, dosimetry, and toxicity of ga-68-nota-anti-her2 nanobodies for ipet imaging of her2 receptor expression in cancer. J Nucl Med 2013; 54: 776–784. doi:10.2967/jnumed.112.111021.
17. Keyaerts M, Xavier C, Heemskerk J, Devoogdt N, Everaert H, Ackaert C, Vanhoeij M, Duhoux FP, Gevaert T, Simon P, Schallier D, Fontaine C, Vaneycken I, Vanhove C, De Greve J, Lamote J, Caveliers V, Lahoutte T. Phase I study of 68ga-her2-nanobody for pet/ct assessment of her2 expression in breast carcinoma. J Nucl Med 2016; 57: 27–33. doi:10.2967/jnumed.115.162024.
18. Vincke C, Loris R, Saerens D, Martinez-Rodriguez S, Muyldermans S, Conrath K. General strategy to humanize a camelid single-domain antibody and identification of a universal humanized nanobody scaffold. J Biol Chem 2009; 284: 3273–3284. doi:10.1074/jbc.M806889200.
19. Randolph TW. The two faces of His-tag: immune response versus ease of protein purification. Biotechnol J 2012; 7: 18–19. doi:10.1002/biot.201100459.
20. Madej MP, Coia G, Williams CC, Caine JM, Pearce LA, Attwood R, Bartone NA, Dolezal O, Nisbet RM, Nuttall SD, Adams TE. Engineering of an anti-epidermal growth factor receptor antibody to single chain format and labeling by Sortase A-mediated protein ligation. Biotechnol Bioeng 2012; 109: 1461–1470. doi:10.1002/bit.24407.
21. Truttmann MC, Wu Q, Stiegeler S, Duarte JN, Ingram J, Ploegh HL. HypE-specific nanobodies as tools to modulate hype-mediated target ampylation. J Biol Chem 2015; 290: 9087–9100. doi:10.1074/jbc.M114.634287.
22. Beerli RR, Hell T, Merkel AS, Grawunder U. Sortase enzyme-mediated generation of site-specifically conjugated antibody drug conjugates with high *in vitro* and *in vivo* potency. PLoS One 2015; 10: e0131177. doi:10.1371/journal.pone.0131177.

23. Kornberger P, Skerra A. Sortase-catalyzed *in vitro* functionalization of a HER2-specific recombinant Fab for tumor targeting of the plant cytotoxin gelonin. MAbs 2014; 6: 354–366. doi:10.4161/mabs.27444.
24. Leung MKM, Hagemeyer CE, Johnston APR, Gonzales C, Kamphuis MMJ, Ardipradja K, Such GK, Peter K, Caruso F. Bio-click chemistry: enzymatic functionalization of pegylated capsules for targeting applications. Angew Chem Int Ed 2012; 51: 7132–7136. doi:10.1002/anie.201203612.
25. Witte MD, Cragnolini JJ, Dougan SK, Yoder NC, Popp MW, Ploegh HL. Preparation of unnatural N-to-N and C-to-C protein fusions. Proc Natl Acad Sci U S A 2012; 109: 11993–11998. doi:10.1073/pnas.1205427109.
26. Chen GY, Li Z, Theile CS, Bardhan NM, Kumar PV, Duarte JN, Maruyama T, Rashidfarrokh A, Belcher AM, Ploegh HL. Graphene oxide nanosheets modified with single-domain antibodies for rapid and efficient capture of cells. Chem 2015; 21: 17178–17183. doi:10.1002/chem.201503057.
27. Ta HT, Prabhu S, Leitner E, Jia F, von Elverfeldt D, Jackson KE, Heidt T, Nair AKN, Pearce H, von zur Muhlen C, Wang X, Peter K, Hagemeyer CE. Enzymatic single-chain antibody tagging a universal approach to targeted molecular imaging and cell homing in cardiovascular disease. Circ Res 2011; 109: 365–373. doi:10.1161/circresaha.111.249375.
28. Wang XW, Hagemeyer CE, Hohmann JD, Leitner E, Armstrong PC, Jia F, Olschewski M, Needles A, Peter K, Ahrens I. Novel single-chain antibody-targeted microbubbles for molecular ultrasound imaging of thrombosis validation of a unique noninvasive method for rapid and sensitive detection of thrombi and monitoring of success or failure of thrombolysis in mice. Circulation 2012; 125: 3117–3126. doi:10.1161/circulationaha.111.030312.
29. Paterson BM, Alt K, Jeffery CM, Price RI, Jagdale S, Rigby S, Williams CC, Peter K, Hagemeyer CE, Donnelly PS. Enzyme-mediated site-specific bioconjugation of metal complexes to proteins: sortase-mediated coupling of copper-64 to a single-chain antibody. Angew Chem Int Ed 2014; 53: 6115–6119. doi:10.1002/anie.201402613.
30. Alt K, Paterson BM, Westein E, Rudd SE, Poniger SS, Jagdale S, Ardipradja K, Connell TU, Krippner GY, Nair AKN, Wang X, Tochon-Danguy HJ, Donnelly PS, Peter K, Hagemeyer CE. A versatile approach for the site-specific modification of recombinant antibodies using a combination of enzyme-mediated bioconjugation and click chemistry. Angew Chem Int Ed 2015; 54: 7515–7519. doi:10.1002/anie.201411507.
31. Rashidian M, Keliher EJ, Bilate AM, Duarte JN, Wojtkiewicz GR, Jacobsen JT, Cragnolini J, Swee LK, Victora GD, Weissleder R, Ploegh HL. Noninvasive imaging of immune responses. Proc Natl Acad Sci U S A 2015; 112: 6146–6151. doi:10.1073/pnas.1502609112.
32. Rashidian M, Keliher EJ, Dougan M, Juras PK, Cavallari M, Wojtkiewicz GR, Jacobsen JT, Edens JG, Tas JMJ, Victora G, Weissleder R, Ploegh H. Use of 18 F-2-fluorodeoxyglucose to label antibody fragments for immuno-positron emission tomography of pancreatic cancer. ACS Cent Sci 2015; 1: 142–147. doi:10.1021/acscentsci.5b00121.
33. Shen B-Q, Xu K, Liu L, Raab H, Bhakta S, Kenrick M, Parsons-Reponte KL, Tien J, Yu S-F, Mai E, Li D, Tibbitts J, Baudys J, Saad OM, Scales SJ, McDonald PJ, Hass PE, Eigenbrot C, Nguyen T, Solis WA, Fuji RN, Flagella KM, Patel D, Spencer SD, Khawli LA, Ebens A, Wong WL, Vandlen R, Kaur S, Sliwkowski MX, Scheller RH, Polakis P, Junutula JR. Conjugation site modulates the *in vivo* stability and therapeutic activity of antibody-drug conjugates. Nat Biotechnol 2012; 30: 184–189. doi:10.1038/nbt.2108.
34. Pillow TH, Tien J, Parsons-Reponte KL, Bhakta S, Li H, Staben LR, Li GM, Chuh J, Fourie-O'Donohue A, Darwish M, Yip V, Liu LN, Leipold DD, Su D, Wu E, Spencer SD, Shen BQ, Xu KY, Kozak KR, Raab H, Vandlen R, Phillips GDL, Scheller RH, Polakis P, Sliwkowski MX, Flygare JA, Junutula JR. Site-specific trastuzumab maytansinoid antibody-drug conjugates with improved therapeutic activity through linker and antibody engineering. J Med Chem 2014; 57: 7890–7899. doi:10.1021/jm500552c.
35. Ton-That H, Liu G, Mazmanian SK, Faull KF, Schneewind O. Purification and characterization of sortase, the transpeptidase that cleaves surface proteins of Staphylococcus aureus at the LPXTG motif. Proc Natl Acad Sci U S A 1999; 96: 12424–12429. doi:10.1073/pnas.96.22.12424.
36. Chen I, Dorr BM, Liu DR. A general strategy for the evolution of bond-forming enzymes using yeast display. Proc Natl Acad Sci U S A 2011; 108: 11399–11404. doi:10.1073/pnas.1101046108.
37. Race PR, Bentley ML, Melvin JA, Crow A, Hughes RK, Smith WD, Sessions RB, Kehoe MA, McCafferty DG, Banfield MJ. Crystal structure of Streptococcus pyogenes sortase A: implications for sortase mechanism. J Biol Chem 2009; 284: 6924–6933. doi:10.1074/jbc.M805406200.
38. Hirakawa H, Ishikawa S, Nagamune T. Design of Ca2 + -independent Staphylococcus aureus sortase A mutants. Biotechnol Bioeng 2012; 109: 2955–2961. doi:10.1002/bit.24585.
39. Cadoo KA, Fornier MN, Morris PG. Biological subtypes of breast cancer: current concepts and implications for recurrence patterns. Q J Nucl Med Mol Im 2013; 57: 312–321.
40. D'Huyvetter M, Vincke C, Xavier C, Aerts A, Impens N, Baatout S, De Raeve H, Muyldermans S, Caveliers V, Devoogdt N, Lahoutte T. Targeted radionuclide therapy with A 177Lu-labeled anti-HER2 nanobody. Theranostics 2014; 4: 708–720. doi:10.7150/thno.8156.
41. Vaneycken I, Devoogdt N, Van Gassen N, Vincke C, Xavier C, Wernery U, Muyldermans S, Lahoutte T, Caveliers V. Preclinical screening of anti-HER2 nanobodies for molecular imaging of breast cancer. FASEB J 2011; 25: 2433–2446. doi:10.1096/fj.10-180331.
42. Xavier C, Devoogdt N, Hernot S, Vaneycken I, D'Huyvetter M, De Vos J, Massa S, Lahoutte T, Caveliers V. Site-specific labeling of his-tagged Nanobodies with 99mTc: a practical guide. Methods Mol Biol 2012; 911: 485–490. doi:10.1007/978-1-61779-968-6_30.
43. D'Huyvetter M, Aerts A, Xavier C, Vaneycken I, Devoogdt N, Gijs M, Impens N, Baatout S, Ponsard B, Muyldermans S, Caveliers V, Lahoutte T. Development of 177Lu-nanobodies for radioimmunotherapy of HER2-positive breast cancer: evaluation of different bifunctional chelators. Contrast Media Mol Imaging 2012; 7: 254–264. doi:10.1002/cmmi.491.
44. Conrath KE, Lauwereys M, Galleni M, Matagne A, Frere JM, Kinne J, Wyns L, Muyldermans S. Beta-lactamase inhibitors derived from single-domain antibody fragments elicited in the Camelidae. Antimicrob Agents Chemother 2001; 45: 2807–2812. doi:10.1128/aac.45.10.2807-2812.2001.
45. Vincke C, Gutierrez C, Wernery U, Devoogdt N, Hassanzadeh-Ghassabeh G, Muyldermans S. Generation of single domain antibody fragments derived from camelids and generation of manifold constructs. Methods Mol Biol 2012; 907: 145–176. doi:10.1007/978-1-61779-974-7_8.
46. Gasteiger E, Hoogland C, Gattiker A, Duvaud S, Wilkins MR, Appel RD, Bairoch A. Protein identification and analysis tools on the expasy server. In Humana, The Proteomics Protocols Handbook, Walker JM (eds). Totowa: Press, 571; 607–2005.
47. Lambert C, Leonard N, De Bolle X, Depiereux E. ESyPred3D: Prediction of proteins 3D structures. Bioinformatics 2002; 18: 1250–1256. doi:10.1093/bioinformatics/18.9.1250.

SUPPORTING INFORMATION

Additional supporting information can be found in the online version of this article at the publisher's web site.